

# Unconditionally maximum bound principle preserving linear schemes for the conservative Allen-Cahn equation with nonlocal constraint

Jingwei Li · Lili Ju · Yongyong Cai · Xinlong Feng

Received: date / Accepted: date

**Abstract** In comparison with the Cahn-Hilliard equation, the classic Allen-Cahn equation satisfies the maximum bound principle (MBP) but fails to conserve the mass along the time. In this paper, we consider the MBP and corresponding numerical schemes for the modified Allen-Cahn equation, which is formed by introducing a nonlocal Lagrange multiplier term to enforce the mass conservation. We first study sufficient conditions on the nonlinear potentials under which the MBP holds and provide some concrete examples of nonlinear functions. Then we propose first and second order stabilized exponential time differencing schemes for time integration, which are linear schemes and unconditionally preserve the MBP in the time discrete level. Convergence of these schemes is analyzed as well as their energy stability. Various two and three dimensional numerical experiments are also carried out to validate the theoretical results and demonstrate the performance of the proposed schemes.

**Keywords** Modified Allen-Cahn equation · maximum bound principle · mass conservation · exponential time differencing · stabilizing technique

**Mathematics Subject Classification (2010)** 35B50 · 65M12 · 35K55 · 65R20

## 1 Introduction

The classic Allen-Cahn equation [1] and Cahn-Hilliard equation [3] are well-known prototypical gradient flows with respect to a given free energy functional:

$$E[u] = \frac{\epsilon^2}{2} (\nabla u, \nabla u) + (F(u), 1) = \int_{\Omega} \left( \frac{\epsilon^2}{2} |\nabla u(\mathbf{x}, t)|^2 + F(u(\mathbf{x}, t)) \right) d\mathbf{x}, \quad (1.1)$$

---

Jingwei Li's work was partially supported by National Natural Science Foundation of China grant 61962056. Lili Ju's work was partially supported by US National Science Foundation grant DMS-1818438 and US Department of Energy grant DE-SC0020270. Yongyong Cai's work was partially supported by National Natural Science Foundation of China grants 11771036 and 91630204. Xinlong Feng's work was partially supported by Research Fund from Key Laboratory of Xinjiang Province grant 2020D04002 and National Natural Science Foundation of China grants U19A2079 and 12071406.

---

Jingwei Li

Laboratory of Mathematics and Complex Systems and School of Mathematical Sciences, Beijing Normal University, Beijing 100875, China

E-mail: jingwei@bnu.edu.cn

Lili Ju (Corresponding author)

Department of Mathematics, University of South Carolina, Columbia, SC 29208, USA

E-mail: ju@math.sc.edu

Yongyong Cai

Laboratory of Mathematics and Complex Systems and School of Mathematical Sciences, Beijing Normal University, Beijing 100875, China

E-mail: yongyong.cai@bnu.edu.cn

Xinlong Feng

College of Mathematics and System Science, Xinjiang University, Urumqi 830046, China

E-mail: fxlmath@xju.edu.cn

where  $u(\mathbf{x}, t)$  is the real-valued unknown function,  $\Omega \subset \mathbb{R}^d$  ( $d = 1, 2, 3$ ) is a bounded domain with Lipschitz boundary  $\partial\Omega$ , and  $(\cdot, \cdot)$  denotes the usual  $L^2$  inner product on  $\Omega$  with the corresponding  $L^2$  norm  $\|\cdot\|_0$ . In the phase-field applications [1, 3] such as two phases material,  $u$  often denotes the phase variable,  $\epsilon > 0$  represents the interface width of the two phases and  $F(u)$  is the associated nonlinear potential function. The Allen-Cahn equation could be viewed as the  $L^2$  (non-conservative form) gradient flow of the energy functional (1.1):

$$\partial_t u(\mathbf{x}, t) = -\frac{\delta E}{\delta u} = \epsilon^2 \Delta u(\mathbf{x}, t) + f(u(\mathbf{x}, t)), \quad \mathbf{x} \in \Omega, \quad t > 0, \quad (1.2)$$

and the Cahn-Hilliard equation could be viewed as the  $H^{-1}$  (conservative form) gradient flow of (1.1),

$$\partial_t u(\mathbf{x}, t) = -\Delta\left(-\frac{\delta E}{\delta u}\right) = -\Delta(\epsilon^2 \Delta u(\mathbf{x}, t) + f(u(\mathbf{x}, t))), \quad \mathbf{x} \in \Omega, \quad t > 0, \quad (1.3)$$

where  $f(u) = -F'(u)$ . One can equip (1.2) and (1.3) with the periodic or homogeneous Neumann boundary condition, which is quite popular in the literature. Under either of these boundary conditions, the following energy dissipation law holds for the Allen-Cahn equation (1.2):

$$\frac{d}{dt} E[u(\mathbf{x}, t)] = - \int_{\Omega} |\partial_t u(\mathbf{x}, t)|^2 d\mathbf{x} \leq 0,$$

and the energy dissipation law for the Cahn-Hilliard equation (1.3) reads

$$\frac{d}{dt} E[u(\mathbf{x}, t)] = - \int_{\Omega} \left| \nabla \frac{\delta E}{\delta u} \right|^2 d\mathbf{x} \leq 0.$$

The classic Cahn-Hilliard equation (1.3) is a fourth-order equation which naturally satisfies the mass conservation of the material components, i.e., the total mass  $\int_{\Omega} u(\mathbf{x}, t) d\mathbf{x}$  is unchanged during evolution [6, 8, 13], however it is often difficult to solve numerically due to the high order spatial derivatives. In contrast, the Allen-Cahn equation (1.2) is second-order and does not satisfy the mass conservation, but it is relatively easier to handle numerically. Moreover, the Allen-Cahn equation possesses some important properties such as maximum bound principle and comparison principle [29]. It is then desirable to also preserve these properties when numerically simulating the dynamics described by the Allen-Cahn equation.

The maximum bound principle (MBP) has become an important mathematics tool to study the physical property of the phase field related equations [12], where MBP means that if the initial data and/or the boundary value are pointwisely bounded by some specific constant in the absolute value, then the absolute value of the solution to the governing equation is also bounded by the same constant for all time. It is well-known that the Cahn-Hilliard equation fails to satisfy MBP due to the fourth order bi-harmonic operator. However, for some models the phase variable would be bounded from above/below by the construction of the free energy. Recently, for the Cahn-Hilliard equation with logarithmic potential function (requires the phase variable to be strictly positive), some positivity preserving numerical schemes [4, 9, 30] were proposed based on the stabilized convex splitting technique. However, these schemes are nonlinear due to the implicit treatment of the nonlinear terms and lead to the need of iterative solver at each time step. In order to decrease the difficulty of numerical solution process and to preserve the bounds of phase variables (usually assumed in modeling), the second-order Allen-Cahn equation has been extensively used in many researches for modeling the dynamical evolution. To further improve the unphysical nonconservative Allen-Cahn dynamics, an alternative choice is the conservative Allen-Cahn equation [5] inspired by the work of Rubinstein and Sternberg [31], where the mass conservation is realized by adding a nonlocal Lagrange multiplier.

During the past decades, there have been many studies devoted to the MBP (or maximum principle) preserving numerical methods for the classical Allen-Cahn equation. For the spatial discretizations, a partial list includes the mass-lumping finite element method [39, 41], finite difference method [43], finite volume method [27, 28], etc. For the temporal integration, the stabilized linear semi-implicit schemes were shown to preserve the MBP unconditionally for the first order scheme and conditionally for the second-order scheme [32, 37, 38, 40]. Some nonlinear second-order MBP-preserving schemes were also constructed for the Allen-Cahn type equations [21, 33]. However, MBP-preserving numerical methods for the conservative Allen-Cahn equation are still rare. The operator splitting method has been proven to unconditionally preserve the MBP by adding a different Lagrange multiplier [17, 18, 26, 36, 45, 46], but it is difficult to obtain the energy dissipation of the conservative Allen-Cahn equation. For the energy dissipation property, there exist quite many effective numerical techniques to obtain energy-stable schemes for solving phase-field models, for

instance, the implicit approach [21], the convex splitting method [4, 9, 30], the linear stabilization approach [35], the invariant energy quadratization (IEQ) method [44] and scalar auxiliary variable (SAV) method [34]. It is worth noting that Yang and his collaborators have developed the SAV schemes to preserve the energy stability for the conservative Allen-Cahn model and many of its variants [47, 48, 49].

The exponential time differencing (ETD) method has been recently proposed to preserve the MBP numerically in combination with the stabilizing technique, which was first proposed in [42] to obtain the numerical energy stability of phase field equations. The ETD schemes are linear schemes based on the variation-of-constants formula/Duhamel principle with the nonlinear terms approximated by polynomial interpolations in time, followed by the exact temporal integration [2, 7, 15, 16]. Therefore, the ETD method is applicable to a large family of semilinear parabolic equations, especially for those with a stiff linear part [15, 20, 22, 24, 25]. The first and second order stabilized ETD schemes have been applied to the nonlocal Allen-Cahn equation and proved to be unconditionally MBP-preserving [11]. Then, an abstract framework on the MBP-preserving stabilized ETD schemes was recently established in [12] for a large class of semilinear parabolic equations. The main object of the current paper is to develop the ETD schemes preserving the MBP unconditionally for the conservative Allen-Cahn equation [5, 31]. Following the framework in [12], we derive the conditions on the nonlinear term  $f$  under which the conservative Allen-Cahn equation satisfies MBP. Based on the stabilizing technique, unconditionally MBP-preserving first and second order ETD schemes will be studied including their convergence analysis and energy stabilities.

The rest of the paper is organized as follows. In Section 2, we review and study some basic assumptions on the nonlinear operators of conservative Allen-Cahn equation so that the MBP can hold. We also present some concrete examples of nonlinear functions satisfying the assumptions. In Section 3, an equivalent form of the conservative Allen-Cahn equation by using the stabilizing technique is derived and proven to admit a unique solution and satisfy the MBP unconditionally. In Section 4, the first and second order ETD schemes for time integration of the stabilized system are constructed, which satisfy the discrete MBP and mass conservation unconditionally. In addition, the convergence and energy stability of the ETD schemes are analyzed. In Section 5, we carry out two and three dimensional numerical experiments to verify the convergence and the MBP-preservation of the proposed schemes and to compare the dynamics of the conservative Allen-Cahn equation with that of the Cahn-Hilliard equation. Finally, some conclusions are drawn in Section 6.

## 2 Preliminaries

In this section, we briefly introduce the conservative Allen-Cahn equation [5, 31] and present the conditions on the nonlinear term under which the MBP holds. We recall the classic Allen-Cahn equation in the form

$$\partial_t u(\mathbf{x}, t) = \epsilon^2 \Delta u(\mathbf{x}, t) + f(u(\mathbf{x}, t)), \quad \mathbf{x} \in \Omega, t > 0, \quad (2.1)$$

and the initial value is given by

$$u(\mathbf{x}, 0) = u_0(\mathbf{x}), \quad \mathbf{x} \in \overline{\Omega}.$$

Here,  $u : \Omega \times [0, +\infty) \rightarrow \mathbb{R}$  is the unknown function,  $\Delta : C^2(\overline{\Omega}) \rightarrow C(\overline{\Omega})$  is the Laplace operator and  $f : \mathbb{R} \rightarrow \mathbb{R}$  is a continuously differentiable nonlinear function. For the boundary conditions, we either enforce the periodic boundary condition (only for a rectangular domain  $\Omega = \prod_{i=1}^d (a_i, b_i)$ ) or the homogeneous Neumann boundary condition given by

$$\frac{\partial u(\mathbf{x}, t)}{\partial \mathbf{n}} = 0, \quad \mathbf{x} \in \partial\Omega, t \geq 0, \quad (2.2)$$

where  $\mathbf{n}$  is the outer unit normal vector on  $\partial\Omega$ . It is well-known from classic analysis [12] that the operator  $\Delta$  generates a contraction semigroup  $\{S_\Delta(t) = e^{t\Delta}\}_{t \geq 0}$  with respect to the supremum norm on the subspace of  $C(\overline{\Omega})$  that satisfies such boundary conditions. For any finite terminal time  $T > 0$ , we denote  $\Omega_T = \Omega \times (0, T)$  and  $C^{2,1}(\Omega_T) = \{v(\mathbf{x}, t) \mid v(\mathbf{x}, \cdot) \in C^1(0, T), \forall \mathbf{x} \in \Omega; v(\cdot, t) \in C^2(\Omega), \forall t \in (0, T)\}$ .

Note that the mass of  $u$  in (2.1) is not conserved, i.e.,  $\frac{d}{dt} \int_\Omega u(\mathbf{x}, t) d\mathbf{x} \neq 0$ , one can impose a nonlocal Lagrange multiplier to conserve the total mass of  $u$ , and the resulting conservative Allen-Cahn equation reads as [31]:

$$\partial_t u(\mathbf{x}, t) = \epsilon^2 \Delta u(\mathbf{x}, t) + \bar{f}[u](\mathbf{x}, t), \quad \mathbf{x} \in \Omega, t > 0, \quad (2.3)$$

where the revised nonlinear term is defined as

$$\bar{f}[u](\mathbf{x}, t) = f(u(\mathbf{x}, t)) - \frac{1}{|\Omega|} \int_{\Omega} f(u(\mathbf{y}, t)) d\mathbf{y} = f(u(\mathbf{x}, t)) - \lambda(t), \quad (2.4)$$

and  $\lambda(t) = \frac{1}{|\Omega|} \int_{\Omega} f(u(\mathbf{y}, t)) d\mathbf{y}$  ( $|\Omega|$  is the Lebesgue measure of  $\Omega$ ) is the Lagrange multiplier for the mass conservation and is independent of  $\mathbf{x}$ .

The modified Allen-Cahn equation (2.3) with nonlocal constraint conserves the mass and satisfies an energy dissipation law. Taking the  $L^2$  inner product with 1 on both sides of (2.3), we obtain

$$\frac{d}{dt} \int_{\Omega} u(\mathbf{x}, t) d\mathbf{x} = 0 \quad \text{and} \quad V(t) = \int_{\Omega} u(\mathbf{x}, t) d\mathbf{x} \equiv V(0) := M, \quad \forall t > 0, \quad (2.5)$$

which means the mass is conserved exactly along the time. Taking the  $L^2$  inner product with  $\partial_t u(\mathbf{x}, t)$  on both sides of (2.3), applying the boundary conditions and integration by parts, we obtain the energy dissipation law as

$$\frac{d}{dt} E[u(\mathbf{x}, t)] = - \int_{\Omega} |\partial_t u(\mathbf{x}, t)|^2 d\mathbf{x} \leq 0,$$

where we have used the identity  $(\bar{f}[u], u_t) = (f(u), u_t)$  deduced from (2.4) and (2.5).

In order to establish MBP for the conservative Allen-Cahn equation (2.3), as well as its time discretizations, we first make the following assumptions on the nonlinear function  $f$ .

**Assumption 1** [31] *There exists a constant  $\beta > 0$  such that*

$$\forall w \in [-\beta, \beta], \quad f(\beta) \leq f(w) \leq f(-\beta). \quad (2.6)$$

*Remark 1* If the function  $f$  only satisfies  $f(M) \leq f(w) \leq f(m)$  for  $w \in [m, M]$  instead of (2.6), by performing the same affine map as in [12], we still can obtain the MBP of the conservative Allen-Cahn equation (2.3).

**Corollary 1** *Under Assumption 1, we can conclude that if  $u(\mathbf{x}, t) \in [-\beta, \beta]$  for all  $\mathbf{x} \in \Omega$ , then*

$$f(\beta) \leq \lambda(t) = \frac{1}{|\Omega|} \int_{\Omega} f(u(\mathbf{y}, t)) d\mathbf{y} \leq f(-\beta).$$

For the Laplace operator  $\Delta$  with the periodic or homogeneous Neumann boundary condition (2.2), following the analysis in [12], we have the lemma below regarding the semigroup generated by  $\Delta - \alpha$  ( $\alpha \geq 0$ ).

**Lemma 2.1** *The Laplace operator  $\Delta$  with the periodic or homogeneous Neumann boundary condition (2.2) generates a contraction semigroup  $\{S_{\Delta}(t) = e^{t\Delta}\}_{t \geq 0}$  with respect to the supremum norm on  $C(\bar{\Omega})$ . Moreover, for  $\alpha \geq 0$ , there holds*

$$\|e^{t(\Delta - \alpha)} u_0\| \leq e^{-\alpha t} \|u_0\|, \quad \forall t \geq 0, u_0 \in C(\bar{\Omega}),$$

where  $\|u_0\| = \max_{\mathbf{x} \in \bar{\Omega}} |u_0(\mathbf{x})|$ .

Next, we introduce the MBP of (2.3) presented in [31].

**Theorem 2.1** [31] *Given a constant  $T > 0$  and assume  $u(\mathbf{x}, t) \in C^{2,1}(\Omega_T) \cap C([0, T]; C^1(\bar{\Omega})) \cap C(\bar{\Omega}_T)$  is the (classical) solution to the conservative Allen-Cahn equation (2.3) with the periodic or homogeneous Neumann boundary condition. If Assumption 1 holds and the initial value satisfies  $|u(\mathbf{x}, 0)| \leq \beta$  for any  $\mathbf{x} \in \bar{\Omega}$ , we have  $|u(\mathbf{x}, t)| \leq \beta$  for any  $(\mathbf{x}, t) \in \bar{\Omega}_T$ .*

## 2.1 Examples of the nonlinear function $f$

In the following, we give some concrete examples of the nonlinear operator satisfying Assumption 1 for the conservative Allen-Cahn equation (2.3).

**Example 1** *The quartic double-well (Ginzburg-Landau) potential function*

$$F(u) = \frac{1}{4}(u^2 - 1)^2, \quad f(u) = -F'(u) = u - u^3. \quad (2.7)$$

Through simple computations, it is easy to see that

$$f'(u) > 0, \quad \forall u \in \left(-\frac{\sqrt{3}}{3}, \frac{\sqrt{3}}{3}\right),$$

see Figure 1-(left), which implies that

$$f(-\beta) \geq f\left(\frac{\sqrt{3}}{3}\right) \text{ and } f(\beta) \leq f\left(-\frac{\sqrt{3}}{3}\right).$$

Consequently, we can find that  $f$  satisfies Assumption 1 for any  $\beta \in [\frac{2}{3}\sqrt{3}, +\infty)$ .

**Example 2** *The Flory-Huggins potential function*

$$F(u) = \frac{\theta}{2}[(1+u)\ln(1+u) + (1-u)\ln(1-u)] - \frac{\theta_c}{2}u^2, \quad f(u) = -F'(u) = \frac{\theta}{2}\ln\frac{1-u}{1+u} + \theta_c u, \quad (2.8)$$

where  $\theta$  and  $\theta_c$  are two constants satisfying  $0 < \theta < \theta_c$ . It is easy to verify that

$$f'(u) > 0, \quad \forall u \in \left(-\sqrt{1 - \frac{\theta}{\theta_c}}, \sqrt{1 - \frac{\theta}{\theta_c}}\right),$$

see Figure 1-(middle), and thus it must hold that

$$f(-\beta) \geq f\left(\sqrt{1 - \frac{\theta}{\theta_c}}\right) \text{ and } f(\beta) \leq f\left(-\sqrt{1 - \frac{\theta}{\theta_c}}\right).$$

Note that  $f(-1) = +\infty$  and  $f(1) = -\infty$ , then we can find that  $f$  defined by (2.8) satisfies Assumption 1 for any  $\beta \in [\gamma, 1)$ , where  $\gamma$  is the positive root of  $f(\gamma) = f\left(-\sqrt{1 - \frac{\theta}{\theta_c}}\right)$ .

**Example 3** *The Lennard-Jones potential function*

$$F(u) = \frac{1}{3}u^{-8} - \frac{4}{3}u^{-2}, \quad f(u) = -F'(u) = -\frac{8}{3}u^{-3} + \frac{8}{3}u^{-9}.$$

It is easy to verify that

$$f'(u) < 0, \quad \forall u \in (0, 3^{1/6}),$$

see Figure 1-(right). Thus  $f$  satisfies the assumption in Remark 1 for  $0 < m < M \leq 3^{1/6}$ .

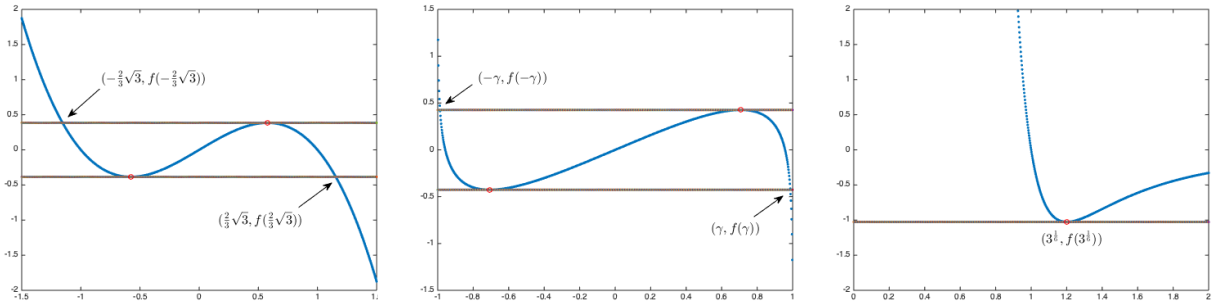


**Fig. 1** Plots of the nonlinear function  $f$  derived from the quartic double-well potential (left), the Flory-Huggins potential (middle) and the Lennard-Jones potential (right), respectively.

### 3 Stabilizing formulation of the conservative Allen-Cahn equation

In this section, we apply the stabilizing technique to obtain an equivalent form of the conservative Allen-Cahn equation (2.3), and then show that it admits a unique solution and satisfies the MBP from this special perspective. This form will also play an important role in designing the desired MBP-preserving schemes in the time discrete setting.

Introducing a stabilizing constant  $\kappa > 0$ , the conservative Allen-Cahn equation (2.3) can be written in the following equivalent form:

$$\partial_t u = \mathcal{L}_\kappa u + \mathcal{N}[u], \quad \mathbf{x} \in \Omega, \quad t > 0, \quad (3.1)$$

where

$$\mathcal{L}_\kappa = \epsilon^2 \Delta - \kappa$$

and

$$\mathcal{N}[u](\mathbf{x}, t) = \kappa u(\mathbf{x}, t) + \bar{f}[u](\mathbf{x}, t) = \kappa u(\mathbf{x}, t) + f(u(\mathbf{x}, t)) - \frac{1}{|\Omega|} \int_{\Omega} f(u(\mathbf{y}, t)) d\mathbf{y}, \quad \mathbf{x} \in \Omega. \quad (3.2)$$

The stabilizing constant  $\kappa$  is chosen such that

$$\kappa \geq \max_{|\eta| \leq \beta} |f'(\eta)|. \quad (3.3)$$

Note that (3.3) is well-defined since  $f$  is continuously differentiable.

**Lemma 3.1** *Under Assumption 1 and the choice of stabilizing constant (3.3), we have*

- (I)  $\|\mathcal{N}[\zeta]\| \leq \kappa\beta$  for any  $\zeta \in C(\bar{\Omega})$  with  $\|\zeta\| \leq \beta$ .
- (II)  $\|\mathcal{N}[\zeta_1] - \mathcal{N}[\zeta_2]\| \leq 3\kappa\|\zeta_1 - \zeta_2\|$ , for any  $\zeta_j \in C(\bar{\Omega})$  with  $\|\zeta_j\| \leq \beta$  ( $j = 1, 2$ ).

*Proof* From (3.3), we have that for any  $\zeta(\mathbf{x}) \in C(\bar{\Omega})$  with  $\zeta \in [-\beta, \beta]$ ,

$$0 \leq \kappa + f'(\zeta(\mathbf{x})) \leq 2\kappa, \quad \forall \mathbf{x} \in \bar{\Omega},$$

and thus

$$-\kappa\beta + f(-\beta) \leq \kappa\zeta(\mathbf{x}) + f(\zeta(\mathbf{x})) \leq \kappa\beta + f(\beta).$$

Using Assumption 1, according to Corollary 1, we further get for any  $\mathbf{x} \in \bar{\Omega}$

$$-\kappa\beta \leq -\kappa\beta + f(-\beta) - \frac{1}{|\Omega|} \int_{\Omega} f(\zeta(\mathbf{y})) d\mathbf{y} \leq \mathcal{N}[\zeta](\mathbf{x}) \leq \kappa\beta + f(\beta) - \frac{1}{|\Omega|} \int_{\Omega} f(\zeta(\mathbf{y})) d\mathbf{y} \leq \kappa\beta,$$

which gives (I). For (II), by the choice of  $\kappa$ , we have that for any  $\mathbf{x} \in \bar{\Omega}$

$$\begin{aligned} |\mathcal{N}[\zeta_1](\mathbf{x}) - \mathcal{N}[\zeta_2](\mathbf{x})| &\leq |\kappa\zeta_1(\mathbf{x}) - \kappa\zeta_2(\mathbf{x}) + f(\zeta_1(\mathbf{x})) - f(\zeta_2(\mathbf{x}))| + \left| \frac{1}{|\Omega|} \int_{\Omega} (f(\zeta_1(\mathbf{y})) - f(\zeta_2(\mathbf{y}))) d\mathbf{y} \right| \\ &\leq 2\kappa|\zeta_1(\mathbf{x}) - \zeta_2(\mathbf{x})| + \frac{1}{|\Omega|} \int_{\Omega} |f(\zeta_1(\mathbf{y})) - f(\zeta_2(\mathbf{y}))| d\mathbf{y} \\ &\leq 2\kappa|\zeta_1(\mathbf{x}) - \zeta_2(\mathbf{x})| + \frac{1}{|\Omega|} \int_{\Omega} \kappa\|\zeta_1 - \zeta_2\| d\mathbf{y} \\ &\leq 3\kappa\|\zeta_1 - \zeta_2\|, \end{aligned}$$

which completes the proof.  $\square$

Now we can show that (3.1) admits a unique solution and possesses the MBP.

**Theorem 3.1** *Under Assumption 1, suppose that the initial value of (3.1) satisfies  $|u_0(\mathbf{x})| \leq \beta$  for any  $\mathbf{x} \in \Omega$  ( $u_0 \in C(\bar{\Omega})$ ) and the equation is equipped with the periodic or homogeneous Neumann boundary condition, then the conservative Allen-Cahn equation (3.1) has a unique solution  $u \in C(\bar{\Omega}_T)$  which satisfies  $|u(\mathbf{x}, t)| \leq \beta$  for any  $(\mathbf{x}, t) \in \bar{\Omega}_T$ .*

*Proof* The proof follows the process presented in [12]. For simplicity, let us consider the case of periodic boundary condition only since the case of homogeneous Neumann condition is similar. Denote  $\mathcal{X}_\beta = \{g(\mathbf{x}) \in C(\overline{\Omega}) \mid \|g\| \leq \beta \text{ and } g \text{ is } \Omega\text{-periodic}\}$ . For a fixed  $t_0 > 0$  and a given  $v := v(\mathbf{x}, t) \in C([0, t_0]; \mathcal{X}_\beta)$ , we define  $w := w(\mathbf{x}, t)$  to be the solution of the following linear problem

$$\begin{cases} w_t = \mathcal{L}_\kappa w + \mathcal{N}[v], & \mathbf{x} \in \Omega, t \in (0, t_0], \\ w(\mathbf{x}, 0) = u_0(\mathbf{x}), & \mathbf{x} \in \overline{\Omega}, \end{cases} \quad (3.4)$$

with the periodic boundary condition. It is easy to see that  $w \in C(\overline{\Omega}_{t_0})$  is uniquely defined due to the linearity of the problem. By Duhamel principle,

$$w(\mathbf{x}, t) = e^{t\mathcal{L}_\kappa} u_0(\mathbf{x}) + \int_0^t e^{(t-s)\mathcal{L}_\kappa} \mathcal{N}[v(\mathbf{x}, s)] ds, \quad \mathbf{x} \in \Omega, t \in (0, t_0]. \quad (3.5)$$

Taking the supremum norm  $\|\cdot\|$  on both sides, using Lemmas 2.1 and 3.1, we have

$$\begin{aligned} \|w(\mathbf{x}, t)\| &\leq e^{-\kappa t} \|u_0\| + \int_0^t e^{-\kappa(t-s)} \|\mathcal{N}[v](\mathbf{x}, s)\| ds \\ &\leq e^{-\kappa t} \beta + \int_0^t e^{-\kappa(t-s)} \kappa \beta ds = \beta, \quad \forall t \in (0, t_0], \end{aligned}$$

which shows  $w \in C([0, t_0]; \mathcal{X}_\beta)$ .

Therefore, from (3.4), we can define the map  $\mathcal{A} : C([0, t_0]; \mathcal{X}_\beta) \rightarrow C([0, t_0]; \mathcal{X}_\beta)$  as  $\mathcal{A}v = w$ . In fact,  $\mathcal{A}$  is a contraction map for sufficiently small  $t_0$ . To see this, setting  $v_1, v_2 \in C([0, t_0]; \mathcal{X}_\beta)$ ,  $w_1 = \mathcal{A}v_1$  and  $w_2 = \mathcal{A}v_2$ , we have from (3.5) that

$$w_1(\mathbf{x}, t) - w_2(\mathbf{x}, t) = \int_0^t e^{(t-s)\mathcal{L}_\kappa} (\mathcal{N}[v_1](\mathbf{x}, s) - \mathcal{N}[v_2](\mathbf{x}, s)) ds.$$

Lemmas 2.1 and 3.1 then imply

$$\begin{aligned} \|w_1 - w_2\|_{C([0, t_0]; C(\overline{\Omega}))} &\leq \int_0^{t_0} e^{-\kappa(t_0-s)} 3\kappa \|v_1 - v_2\|_{C([0, t_0]; C(\overline{\Omega}))} ds \\ &= 3(1 - e^{-\kappa t_0}) \|v_1 - v_2\|_{C([0, t_0]; C(\overline{\Omega}))}. \end{aligned}$$

Thus, for  $t_0 < \kappa^{-1} \ln \frac{3}{2}$  such that  $3(1 - e^{-\kappa t_0}) < 1$ ,  $\mathcal{A}$  becomes a contraction map. Since  $\mathcal{X}_\beta$  is closed in  $C(\overline{\Omega})$ , we know that  $C([0, t_0]; \mathcal{X}_\beta)$  is complete with respect to the metric induced by the norm  $\|\cdot\|_{C([0, t_0]; C(\overline{\Omega}))}$ . Banach's fixed point theorem would yield that  $\mathcal{A}$  has a unique fixed point in  $C([0, t_0]; \mathcal{X}_\beta)$ , which is the solution to the conservative Allen-Cahn equation (3.1). Continuing the iteration, the solution can be extended to entire time domain  $[0, +\infty)$ , and in particular  $u \in C([0, T]; \mathcal{X}_\beta)$  (see [12] for more discussions).  $\square$

## 4 Exponential time differencing schemes for temporal approximation

In this section, we recall the construction of the exponential time differencing (ETD) schemes for the model equation (2.3) following the abstract framework in [12]. The first and second order ETD schemes with the unconditional MBP-preserving property will be discussed based on the equivalent form (3.1) as well as the convergences and energy stabilities.

### 4.1 ETD schemes, mass conservation and discrete MBP

Given a time step size  $\tau > 0$ , we divide the total time by  $\{t^n = n\tau\}_{n \geq 0}$ . To establish the ETD schemes for the conservative Allen-Cahn equation (3.1) on the time interval  $[t^n, t^{n+1}]$ , we start with the exact solution  $w(\mathbf{x}, s) = u(\mathbf{x}, t^n + s)$  satisfying

$$\begin{cases} \partial_s w = \mathcal{L}_\kappa w + \mathcal{N}[w], & \mathbf{x} \in \Omega, s \in (0, \tau], \\ w(\mathbf{x}, 0) = u(\mathbf{x}, t^n), & \mathbf{x} \in \overline{\Omega}, \end{cases} \quad (4.1)$$

subject to the periodic or homogeneous Neumann boundary condition. The first order ETD (ETD1) scheme is then followed by setting  $\mathcal{N}[u(t^n + s)] \approx \mathcal{N}[u(t^n)]$  in (4.1) which has a truncation error of  $O(\tau)$ , i.e., for  $n \geq 0$  and given  $u^0(\mathbf{x}) = u_0(\mathbf{x})$ , find  $u^{n+1} = w^n(\tau)$  by solving

$$\begin{cases} \partial_s w^n = \mathcal{L}_\kappa w^n + \mathcal{N}[u^n], & \mathbf{x} \in \Omega, s \in (0, \tau], \\ w^n(\mathbf{x}, 0) = u^n(\mathbf{x}), & \mathbf{x} \in \overline{\Omega}. \end{cases} \quad (4.2)$$

**Lemma 4.1** (*Mass conservation of ETD1*). *The ETD1 scheme (4.2) conserves the mass unconditionally at the time discrete level, i.e., for any time step size  $\tau > 0$ , the ETD1 solution satisfies*

$$\int_{\Omega} u^{n+1} d\mathbf{x} = \int_{\Omega} u^n d\mathbf{x} = \dots = \int_{\Omega} u^0 d\mathbf{x} := M, \quad \forall n \geq 0.$$

*Proof* We just need to show that  $\int_{\Omega} u^n d\mathbf{x} = M$  implies  $\int_{\Omega} u^{n+1} d\mathbf{x} = M$ . Taking  $L^2$  inner product with 1 on both sides of (4.2) and noticing the properties of  $\mathcal{N}[u]$ , we have

$$\frac{d}{ds} \int_{\Omega} w^n(\mathbf{x}, s) d\mathbf{x} + \kappa \int_{\Omega} w^n(\mathbf{x}, s) d\mathbf{x} = \kappa \int_{\Omega} u^n d\mathbf{x} = \kappa M,$$

which implies the quantity  $V(s) = \int_{\Omega} w^n(\mathbf{x}, s) d\mathbf{x}$  satisfies the ODE

$$\frac{dV(s)}{ds} + \kappa V(s) = \kappa M, \quad V(0) = M.$$

It is easy to check  $V(s) \equiv M$  is the unique solution to the above ODE. Therefore, we have  $V(\tau) = M$ , that is,  $\int_{\Omega} u^{n+1}(\mathbf{x}) d\mathbf{x} = M$ .  $\square$

**Theorem 4.1** (*Discrete MBP of ETD1*). *Under Assumption 1, the ETD1 scheme (4.2) preserves the discrete MBP unconditionally, i.e., for any time step size  $\tau > 0$ , the numerical solution  $u^n$  ( $n \geq 1$ ) obtained by ETD1 (4.2) satisfies  $\|u^n\| \leq \beta$  if the initial value  $u^0 = u_0(\mathbf{x}) \in C(\overline{\Omega})$  satisfies  $\|u^0\| \leq \beta$ .*

*Proof* It suffices to prove  $\|u^{n+1}\| \leq \beta$  if  $\|u^n\| \leq \beta$ . From ETD1 (4.2), we have

$$u^{n+1} = e^{\tau \mathcal{L}_\kappa} u^n + \int_0^\tau e^{(\tau-s)\mathcal{L}_\kappa} \mathcal{N}[u^n] ds.$$

Using Lemmas 2.1 and 3.1, for  $\|u^n\| \leq \beta$  we have

$$\begin{aligned} \|u^{n+1}\| &\leq e^{-\kappa\tau} \|u^n\| + \int_0^\tau e^{-\kappa(\tau-s)} \kappa \beta ds \\ &\leq \beta e^{-\kappa\tau} + \kappa \beta \frac{1 - e^{-\kappa\tau}}{\kappa} = \beta, \end{aligned}$$

which verifies the MBP-preserving property of ETD1 (4.2).  $\square$

Next, we consider the second order temporal approximation of the solution to (4.1) by setting

$$\mathcal{N}[u(t^n + s)] \approx (1 - \frac{s}{\tau})\mathcal{N}[u(t^n)] + \frac{s}{\tau}\mathcal{N}[u(t^{n+1})],$$

which has a truncation error of  $O(\tau^2)$ . The corresponding second order ETD Runge-Kutta (ETDRK2) scheme then can be constructed as follows: for  $n \geq 0$  and given  $u^0 = u_0(\mathbf{x})$ , find  $u^{n+1} = w^n(\tau)$  by solving

$$\begin{cases} \partial_s w^n(\mathbf{x}, s) = \mathcal{L}_\kappa w^n + (1 - \frac{s}{\tau})\mathcal{N}[u^n] + \frac{s}{\tau}\mathcal{N}[\tilde{u}^{n+1}], & \mathbf{x} \in \Omega, s \in (0, \tau], \\ w^n(\mathbf{x}, 0) = u^n, & \mathbf{x} \in \overline{\Omega}, \end{cases} \quad (4.3)$$

where the periodic or homogeneous Neumann boundary condition is imposed and  $\tilde{u}^{n+1}$  is generated by the ETD1 scheme (4.2) from  $u^n$ . It is worth noting that both ETD1 and ETDRK2 schemes are linear.

**Lemma 4.2** (Mass conservation of ETDRK2). *The ETDRK2 scheme (4.3) conserves the mass unconditionally at the time discrete level, i.e., for any time step size  $\tau > 0$ , the ETDRK2 solution satisfies*

$$\int_{\Omega} u^{n+1} d\mathbf{x} = \int_{\Omega} u^n d\mathbf{x} = \dots = \int_{\Omega} u^0 d\mathbf{x} := M, \quad \forall n \geq 0.$$

*Proof* Similar to the proof in Lemma 4.1, taking the  $L^2$  inner product with 1 on both sides of (4.3), we have

$$\frac{d}{ds} \int_{\Omega} w^n(\mathbf{x}, s) d\mathbf{x} + \kappa \int_{\Omega} w^n(\mathbf{x}, s) d\mathbf{x} = (1 - \frac{s}{\tau})\kappa \int_{\Omega} u^n d\mathbf{x} + \frac{s}{\tau}\kappa \int_{\Omega} \bar{u}^{n+1} d\mathbf{x} = \kappa M, \quad s \in (0, \tau],$$

where we have used  $\int_{\Omega} \bar{u}^{n+1} d\mathbf{x} = M$  from Lemma 4.1. Using the same arguments in Lemma 4.1, we can obtain that  $\int_{\Omega} u^{n+1} d\mathbf{x} = \int_{\Omega} w^n(\mathbf{x}, \tau) d\mathbf{x} = M$ .  $\square$

**Theorem 4.2** (Discrete MBP of ETDRK2). *Under Assumption 1, the ETDRK2 scheme (4.3) preserves the discrete MBP unconditionally, i.e., for any time step size  $\tau > 0$ , the numerical solution  $u^n$  ( $n \geq 1$ ) obtained by ETDRK2 (4.3) satisfies  $\|u^n\| \leq \beta$  ( $n \geq 1$ ) if the initial value  $u^0 = u_0(\mathbf{x}) \in C(\bar{\Omega})$  satisfies  $\|u^0\| \leq \beta$ .*

*Proof* Again, it suffices to prove  $\|u^{n+1}\| \leq \beta$  if  $\|u^n\| \leq \beta$ . From Theorem 4.1, we have  $\|\tilde{u}^{n+1}\| \leq \beta$ . In addition, (4.3) gives

$$u^{n+1} = e^{\tau \mathcal{L}_{\kappa}} u^n + \int_0^{\tau} e^{(\tau-s)\mathcal{L}_{\kappa}} \left( (1 - \frac{s}{\tau})\mathcal{N}[u^n] + \frac{s}{\tau}\mathcal{N}[\tilde{u}^{n+1}] \right) ds.$$

Using Lemmas 2.1 and 3.1, for  $\|u^n\| \leq \beta$  we have

$$\begin{aligned} \|u^{n+1}\| &\leq e^{-\kappa\tau} \|u^n\| + \int_0^{\tau} e^{-\kappa(\tau-s)} \left( (1 - \frac{s}{\tau})\|\mathcal{N}[u^n]\| + \frac{s}{\tau}\|\mathcal{N}[\tilde{u}^{n+1}]\| \right) ds \\ &\leq e^{-\kappa\tau} \beta + \int_0^{\tau} e^{-\kappa(\tau-s)} \kappa \beta ds = \beta, \end{aligned}$$

and the MBP-preserving property of ETDRK2 (4.3) follows.  $\square$

*Remark 2* Under the analysis framework of [12], Theorem 3.1 on the MBP property can be further extended to the case when the differential operator is replaced by certain finite dimensional discrete operators in space, such as discrete approximations of  $\Delta$ , denoted by  $\Delta_h$ , in which the domain of a function is the set of all spatial grid points (boundary and interior points), denoted by  $X$ . The corresponding space-discrete equation of (4.1) with  $\Delta_h$  becomes an ordinary differential equation (ODE) system taking the same form:

$$u_t = \epsilon^2 \Delta_h u + \bar{f}[u], \quad \mathbf{x} \in X^*, t > 0$$

with  $u(\mathbf{x}, 0) = u_0(\mathbf{x})$ , where  $X^* = X$  for the homogeneous Neumann boundary condition and  $X^* = X \cap \bar{\Omega}^+$  with  $\bar{\Omega}^+ = \prod_{i=1}^d (a_i, b_i]$  for the periodic boundary condition. As shown in [12], it is easy to verify that the central finite difference operator and finite element operator with lumped mass in the space-discrete case discretizing the Laplace operator  $\Delta$  satisfy Lemma 2.1. In our discussion,  $\Delta_h$  can be simply regarded as a square matrix and the contraction semigroup  $\{S_{\Delta_h}(t) = e^{t\Delta_h}\}$  can be viewed as a matrix exponential. Let  $\mathcal{L}_{\kappa,h} = \epsilon^2 \Delta_h - \kappa \mathcal{I}$  and define the  $\phi$ -functions as follows:

$$\phi_0(z) = e^z, \quad \phi_1(z) = \frac{e^z - 1}{z}, \quad \phi_2(z) = \frac{e^z - z - 1}{z^2}.$$

We then can write down the equivalent integral forms of ETD1 (4.2) and ETDRK2 (4.3) used in practical computations. The corresponding fully discrete ETD1 scheme of (4.2) is given by

$$u^{n+1} = \phi_0(\tau \mathcal{L}_{\kappa,h}) u^n + \tau \phi_1(\tau \mathcal{L}_{\kappa,h}) \mathcal{N}[u^n], \quad (4.4)$$

and the corresponding fully discrete ETDRK2 scheme of (4.3) reads

$$\begin{cases} \bar{u}^{n+1} = \phi_0(\tau \mathcal{L}_{\kappa,h}) u^n + \tau \phi_1(\tau \mathcal{L}_{\kappa,h}) \mathcal{N}[u^n], \\ u^{n+1} = \bar{u}^{n+1} + \tau \phi_2(\tau \mathcal{L}_{\kappa,h}) (\mathcal{N}[\bar{u}^{n+1}] - \mathcal{N}[u^n]). \end{cases} \quad (4.5)$$

Note that the corresponding semigroup is given by the matrix exponential  $S_{\mathcal{L}_{\kappa,h}}(t) = \phi_0(t \mathcal{L}_{\kappa,h})$ , which depends crucially on the choice of the stabilizing coefficient  $\kappa$ .

*Remark 3* As shown in [12], discretization of the spatial operator  $\mathcal{L}$  by the central finite difference method or the lumped-mass finite element method satisfies Lemma 2.1 in the space-discrete sense since the resulting discrete system gives an M-matrix, and therefore the fully discrete ETD1 and ETDRK2 schemes are guaranteed to be unconditionally MBP-preserving. However, the coefficient matrix produced by the Fourier pseudo-spectral method is usually not an M-matrix and then the current analysis framework does not apply. It still remains an open question whether such requirement (Lemma 2.1) is necessary for the space-discrete system to possess unconditional preservation of MBP. In addition, the discrete mass conservation holds for any of the three types of spatial discretizations in the fully discrete ETD1 and ETDRK2 schemes.

#### 4.2 Convergence analysis and energy stability

As an important application of the MBP-preserving property, we now consider the convergence of the ETD1 and ETDRK2 schemes. Since the proof can be concluded in a quite similar way as done in [12], we only state the main results for the ETD1 (4.2) and ETDRK2 (4.3) schemes. The key point is that the MBP property ensures *a priori*  $L^\infty$  bounds on the numerical solutions, which greatly reduces the difficulty of convergence analysis.

**Theorem 4.3** *Under Assumption 1, for a fixed terminal time  $T > 0$ , assume that the exact solution  $u(\mathbf{x}, t)$  to the conservative Allen-Cahn equation (3.1) belongs to  $C^1([0, T]; C(\bar{\Omega}))$  and the initial value  $u_0(\mathbf{x})$  satisfies  $\|u_0\| \leq \beta$ , and let  $\{u^n\}_{n \geq 0}$  be generated by the ETD1 scheme (4.2) with  $u^0 = u_0(\mathbf{x})$ , we then have that for any  $\tau > 0$ ,*

$$\|u(t^n) - u^n\| \leq Ce^{2\kappa t^n} \tau, \quad \forall t^n \leq T,$$

where the constant  $C > 0$  is independent of  $\tau$  and  $\kappa$ .

**Theorem 4.4** *Under Assumption 1, for a fixed terminal time  $T > 0$ , assume that the exact solution  $u(\mathbf{x}, t)$  to the conservative Allen-Cahn equation (3.1) belongs to  $C^2([0, T]; C(\bar{\Omega}))$  and the initial value  $u_0(\mathbf{x})$  satisfies  $\|u_0\| \leq \beta$ , and let  $\{u^n\}_{n \geq 0}$  be generated by the ETDRK2 scheme (4.3) with  $u^0 = u_0(\mathbf{x})$ , we then have that for any  $\tau > 0$ ,*

$$\|u(t^n) - u^n\| \leq Ce^{2\kappa t^n} \tau^2, \quad \forall t^n \leq T,$$

where the constant  $C > 0$  is independent of  $\tau$ .

As shown in the abstract framework [12], the ETD1 (4.2) and ETDRK2 (4.3) schemes for (3.1) still enjoy the energy stabilities. Here, we consider the energy (1.1) for the semi-discrete ETD1 and ETDRK2 schemes. The following lemma regarding the energy (1.1) is useful.

**Lemma 4.3** *Under Assumption 1, for any  $v(\mathbf{x}), w(\mathbf{x}) \in C(\bar{\Omega}) \cap H^1(\Omega)$  satisfying  $\|w\| \leq \beta$ ,  $\|v\| \leq \beta$  and  $\int_{\Omega} v(\mathbf{x}) d\mathbf{x} = \int_{\Omega} w(\mathbf{x}) d\mathbf{x}$ , and the periodic or homogeneous Neumann boundary condition, it holds that for the energy functional defined by (1.1),*

$$E[v] - E[w] \leq -(\mathcal{L}_\kappa v + \mathcal{N}[w], v - w). \quad (4.6)$$

*Proof* By direct computation and  $f(u) = -F'(u)$ , we find

$$\begin{aligned} E[v] - E[w] &= \frac{\epsilon^2}{2} \int_{\Omega} (|\nabla v|^2 - |\nabla w|^2) d\mathbf{x} + (F(v) - F(w), 1) \\ &= -\frac{\epsilon^2}{2} \|\nabla(v - w)\|_0^2 - (\epsilon^2 \Delta v, v - w) - \int_{\Omega} \int_0^1 f(\theta v + (1 - \theta)w) d\theta (v - w) d\mathbf{x} \\ &\leq -(\mathcal{L}_\kappa v, v - w) - \kappa(v, v - w) - (f(w), v - w) \\ &\quad - \int_{\Omega} \int_0^1 (f(\theta v + (1 - \theta)w) - f(w)) d\theta (v - w) d\mathbf{x} \\ &\leq -(\mathcal{L}_\kappa v, v - w) - (f(w) + \kappa w, v - w) - \kappa(v - w, v - w) \\ &\quad + \int_{\Omega} \int_0^1 \theta \kappa (v - w)^2 d\theta d\mathbf{x} \\ &\leq -(\mathcal{L}_\kappa v, v - w) - (f(w) + \kappa w, v - w) - \frac{\kappa}{2} \|v - w\|_0^2, \end{aligned} \quad (4.7)$$

where we have used the fact that for any  $\theta \in [0, 1]$ , there exists some constant  $\theta_1 \in [0, \theta]$  such that

$$\begin{aligned} -(f(\theta v + (1 - \theta)w) - f(w))(v - w) &= -f'(\theta_1 v + (1 - \theta_1)w)\theta(v - w)(v - w) \\ &\leq \theta\kappa(v - w)^2. \end{aligned}$$

Since  $v$  and  $w$  have equal total mass on  $\Omega$ , we have from (3.2) that for  $\lambda = \frac{1}{|\Omega|} \int_{\Omega} f(w(\mathbf{x})) d\mathbf{x}$ ,

$$(f(w) + \kappa w, v - w) = (f(w) + \kappa w - \lambda, v - w) = (\mathcal{N}[w], v - w).$$

Combining the above identity with (4.7), we finally obtain (4.6).  $\square$

Similar to the results in [11], we have the following discrete energy stabilities for the ETD1 and ETDRK2 schemes.

**Theorem 4.5** *Under Assumption 1, assume initial value  $u^0 = u_0(\mathbf{x}) \in C(\overline{\Omega}) \cap H^1(\Omega)$  with  $\|u_0\| \leq \beta$ , the numerical solution sequence  $\{u^n\}_{n \geq 0}$  generated by the ETD1 scheme (4.2) satisfies*

$$E[u^{n+1}] \leq E[u^n], \quad \forall n \geq 0,$$

for any  $\tau > 0$ , i.e., the ETD1 scheme (4.2) is unconditionally energy stable.

*Proof* For  $u^0 \in C(\overline{\Omega}) \cap H^1(\Omega)$ , we have  $u^n \in C(\overline{\Omega}) \cap H^1(\Omega)$  ( $n \geq 1$ ) so that the energy (1.1) is well-defined. It suffices to consider the energy changes in the interval  $[t^n, t^{n+1}]$ . From the mass conservation (Lemma 4.1) and the discrete MBP (Theorem 4.1) of ETD1, we can apply Lemma 4.3 to obtain

$$E[u^{n+1}] - E[u^n] \leq -(\mathcal{L}_\kappa u^{n+1} + \mathcal{N}[u^n], u^{n+1} - u^n). \quad (4.8)$$

From the integral form (4.4) of ETD1 (4.2), using the stabilizing coefficient  $\kappa$  which ensures  $e^{\tau \mathcal{L}_\kappa} - \mathcal{I}$  is invertible [11], we have

$$\mathcal{N}[u^n] = (e^{\tau \mathcal{L}_\kappa} - \mathcal{I})^{-1} \mathcal{L}_\kappa (u^{n+1} - e^{\tau \mathcal{L}_\kappa} u^n)$$

and

$$\begin{aligned} \mathcal{L}_\kappa u^{n+1} + \mathcal{N}[u^n] &= (e^{\tau \mathcal{L}_\kappa} - \mathcal{I})^{-1} \mathcal{L}_\kappa (u^{n+1} - e^{\tau \mathcal{L}_\kappa} u^n) \\ &= \mathcal{L}_\kappa (u^{n+1} - u^n) + (e^{\tau \mathcal{L}_\kappa} - \mathcal{I})^{-1} \mathcal{L}_\kappa (u^{n+1} - u^n). \end{aligned}$$

Plugging the above identity into (4.8), we arrive at

$$E[u^{n+1}] - E[u^n] \leq -(\mathcal{T}(u^{n+1} - u^n), u^{n+1} - u^n),$$

where  $\mathcal{T} = \mathcal{L}_\kappa + (e^{\tau \mathcal{L}_\kappa} - \mathcal{I})^{-1} \mathcal{L}_\kappa$  is positive-definite [11] ( $\mathcal{L}_\kappa$  here is understood as the self-adjoint expansion of  $\epsilon^2 \Delta - \kappa$  with respect to the boundary conditions) by looking at the function  $s + (e^{\tau s} - 1)^{-1} s = se^{\tau s} / (e^{\tau s} - 1) > 0$  ( $s \in (-\infty, 0)$ ). Hence, we conclude that  $E[u^{n+1}] \leq E[u^n]$ .  $\square$

For the ETDRK2 scheme (4.3), we do not have the energy decaying property, but the following energy bounds could be established [12].

**Theorem 4.6** *Under the assumptions of Theorem 4.4, the numerical solutions  $\{u^n\}_{n \geq 0}$  of the ETDRK2 scheme (4.3) satisfy*

$$E[u^n] \leq E[u^0] + C, \quad t^n \leq T,$$

for any  $\tau \in (0, 1]$ , where the constant  $C$  is independent of  $\tau$ , i.e., the energy is uniformly bounded.

*Proof.* The proof can be proceeded in the same way as in [11, 12] and is omitted here for brevity.  $\square$

*Remark 4* Though we only present the convergence results for the semi-discrete schemes (4.2) and (4.3), these error estimates can be similarly generalized to the fully discrete cases (4.4) and (4.5) by using the discrete MBP-preserving properties. As in the proofs of Theorems 4.5 and 4.6, only  $L^2$  inner products and the maximum bounds of the numerical solutions are used essentially, thus these results also hold for the fully discrete forms of ETD1 (4.4) and ETDRK2 (4.5) under suitable spatial discretizations.

## 5 Numerical experiments

In this section, we present various two-dimensional and three-dimensional numerical examples to demonstrate the accuracies and the MBP preserving properties of the proposed stabilized ETD schemes. In all examples, we set the computational domain  $\Omega = [-0.5, 0.5]^2$  in two dimensions or  $\Omega = [-0.5, 0.5]^3$  in three dimensions. The spatial discretization is realized by the central finite difference method and the products of matrix exponentials with vectors are implemented by the fast Fourier transform (FFT). Moreover, the ETD RK2 (4.5) (or (4.3)) scheme is used for all examples while the ETD1 scheme (4.4) (or (4.2)) is only tested in the temporal convergence test due to its low accuracy. For simplicity, we only test the case of periodic boundary condition, and that of the homogeneous Neumann boundary condition is quite similar. Uniform mesh distribution in each direction is adopted, i.e. spatial mesh size  $h_x = h_y = h = \frac{1}{N}$  in two dimensions and  $h_x = h_y = h_z = h = \frac{1}{N}$  in three dimensions, where  $h$  is the mesh size and  $N$  is the number of grid points in each direction. We denote the corresponding set of discrete grid points as  $\Omega_h$ .

### 5.1 Convergence tests

We consider the conservative Allen-Cahn equation (2.3) in two dimensions with  $\epsilon = 0.01$  and  $f$  defined by (2.7), i.e., the double-well potential function. The initial value is given by

$$u_0(x, y) = \cos(2\pi x) \cos(2\pi y), \quad (x, y) \in \Omega.$$

The terminal time is set to be  $T = 1$  and the stabilizing parameter is chosen as  $\kappa = 3$ .

First, by setting the spatial mesh size to be very fine  $h_e = 1/2048$  such that the spatial discretization error could be ignored, we test the convergence of the proposed schemes in time with various time step sizes. Let  $u_{\tau, h}(t)$  be the numerical solution (understood on the grid points) at time  $t$  obtained by the numerical schemes with the mesh size  $h$  and the time step  $\tau$ . To quantify the errors, the ‘exact’ or say ‘benchmark’ solution is produced by the ETD RK2 scheme with a very fine time step size  $\tau_e = T/1024$ . The error function at time  $T = 1$  of the numerical solution is denoted as

$$e_{\tau, h}(x, y, t = T) := u_{\tau, h}(x, y, t = T) - u_{\tau_e, h_e}(x, y, t = T), \quad (x, y) \in \Omega_h.$$

The  $L^2$  norm and the  $L^\infty$  norm of the error function  $e_{\tau, h_e}(t = T)$  along the uniform refinement of the time step size  $\tau$  and corresponding convergence rates for the fully discrete ETD1 and ETD RK2 schemes are reported in Table 1, where the expected temporal convergence rates (1 for ETD1 and 2 for ETD RK2) are clearly observed.

**Table 1** Temporal errors  $e_{\tau, h_e}(t = T)$  in the  $L^2$  and  $L^\infty$  norms as well as corresponding convergence rates for the fully discrete ETD1 and ETD RK2 schemes.

$\tau$	ETD1				ETD RK2			
	$L^2$ Error	Rate	$L^\infty$ Error	Rate	$L^2$ Error	Rate	$L^\infty$ Error	Rate
$T/4$	5.4448e-2	-	9.1469e-2	-	1.3276e-2	-	2.3360e-2	-
$T/8$	2.9502e-2	0.88	5.0611e-2	0.85	4.0335e-3	1.71	7.1919e-3	1.69
$T/16$	1.5278e-2	0.94	2.6529e-2	0.93	1.1189e-3	1.85	2.0072e-3	1.84
$T/32$	7.6819e-3	0.99	1.3427e-2	0.98	2.9501e-4	1.92	5.3073e-4	1.91
$T/64$	3.7574e-3	1.03	6.5901e-3	1.02	7.5584e-5	1.96	1.3616e-4	1.96
$T/128$	1.7630e-3	1.09	3.0974e-3	1.08	1.8933e-5	1.99	3.4127e-5	1.99
$T/256$	7.5760e-4	1.21	1.3322e-3	1.21	4.5387e-6	2.06	8.1836e-6	2.06

Next, we test the convergence with respect to the spatial mesh size  $h$  by fixing the temporal step size  $\tau = \tau_e$  so that the temporal error could be ignored. The numerical solution obtained by the ETD RK2 scheme with  $h = 1/2048$  is treated as the benchmark for computing the errors of the numerical solutions obtained with various mesh sizes. The numerical errors along the spatial mesh refinement and corresponding convergence rates are presented in Table 2. It is observed that the convergence rates with respect to  $h$  are clearly of second order, which is consistent with the central finite difference stencil as expected.

**Table 2** Spatial errors  $e_{\tau_e, h}(t = T)$  in the  $L^2$  and  $L^\infty$  norms as well as corresponding convergence rates for the fully discrete ETDRK2 scheme.

$1/h$	$L^2$ Error	Rate	$L^\infty$ Error	Rate
64	3.1368e-4	-	9.9889e-4	-
128	9.2116e-5	1.76	3.0942e-4	1.69
256	2.4023e-5	1.93	8.3780e-5	1.88
512	6.0713e-6	1.98	2.1247e-5	1.97
1024	1.5220e-6	1.99	5.3332e-6	1.99

## 5.2 MBP tests and comparisons

We now numerically simulate long-time phase separation processes governed by the conservative Allen-Cahn equation (2.3) and investigate the preservation of discrete MBP. Note that the ETDRK2 scheme is used for all following simulations. We start with the same initial configuration at  $t = 0$ , which is generated by taking  $u_0 = 0.9 \mathbf{rand}(\cdot)$ , where  $\mathbf{rand}(\cdot)$  represents the random distribution between  $-1$  and  $1$ . Here, we consider two different potential functions, i.e., the double-well potential function (2.7) and the Flory-Huggins potential function (2.8).

### 5.2.1 Two-dimensional coarsening

We simulate the conservative Allen-Cahn equation (2.3) with  $\epsilon = 0.01$  in two dimensions, and also compare them with the results obtained by solving the classic Cahn-Hilliard equation with the ETDRK2 scheme as proposed in [24]. The spatial mesh size is chosen to be  $h = 1/1024$ .

We first take  $f$  to be the double-well potential function (2.7) and the stabilizing coefficient is set to be  $\kappa = 3$  correspondingly. Figure 1 shows the configurations of the numerical solution at  $t = 1, 10, 50, 1800$  for the conservative Allen-Cahn equation with different time step sizes  $\tau = 0.1$  and  $\tau = 1$ , respectively. The corresponding evolutions of the mass, the supremum norm and the energy of the numerical solutions are shown in Figure 2, where the red line is the theoretical bound  $\beta = \frac{2}{3}\sqrt{3}$ . We observe that the mass is conserved very well and the energy decays monotonically. Moreover, the discrete MBP is preserved numerically for the conservative Allen-Cahn equation and is close to  $\|u\| = 1$  in time which is the bounding constant of the classic Allen-Cahn equation (1.2). Two simulations produced by different time step sizes give us overall similar evolution processes. The results of the Cahn-Hilliard equation with  $\tau = 0.1$  are presented for  $t = 1, 10, 50, 300$  in Figure 3, where the almost same steady state as that of the conservative Allen-Cahn equation is reached in the end. On the other hand, it is also easy to see that the evolution of the phase structure in the conservative Allen-Cahn equation is slower than that in the Cahn-Hilliard equation.

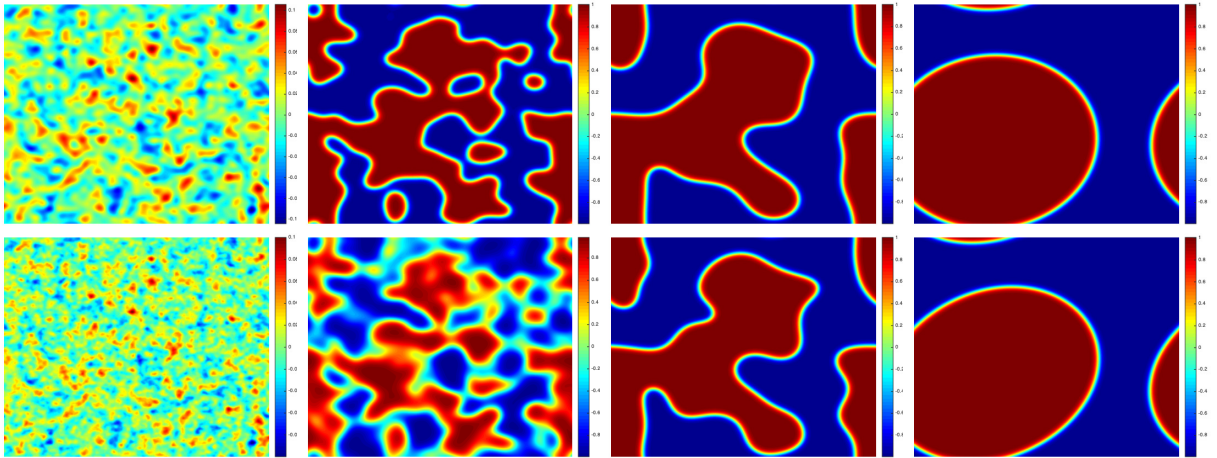


**Fig. 1** Simulated phase structures at  $t = 1, 10, 50, 1800$  (from left to right) with different time step sizes for the conservative Allen-Cahn equation (2.3) with the double-well potential in two dimensions. Top:  $\tau = 0.1$ ; bottom:  $\tau = 1$ .

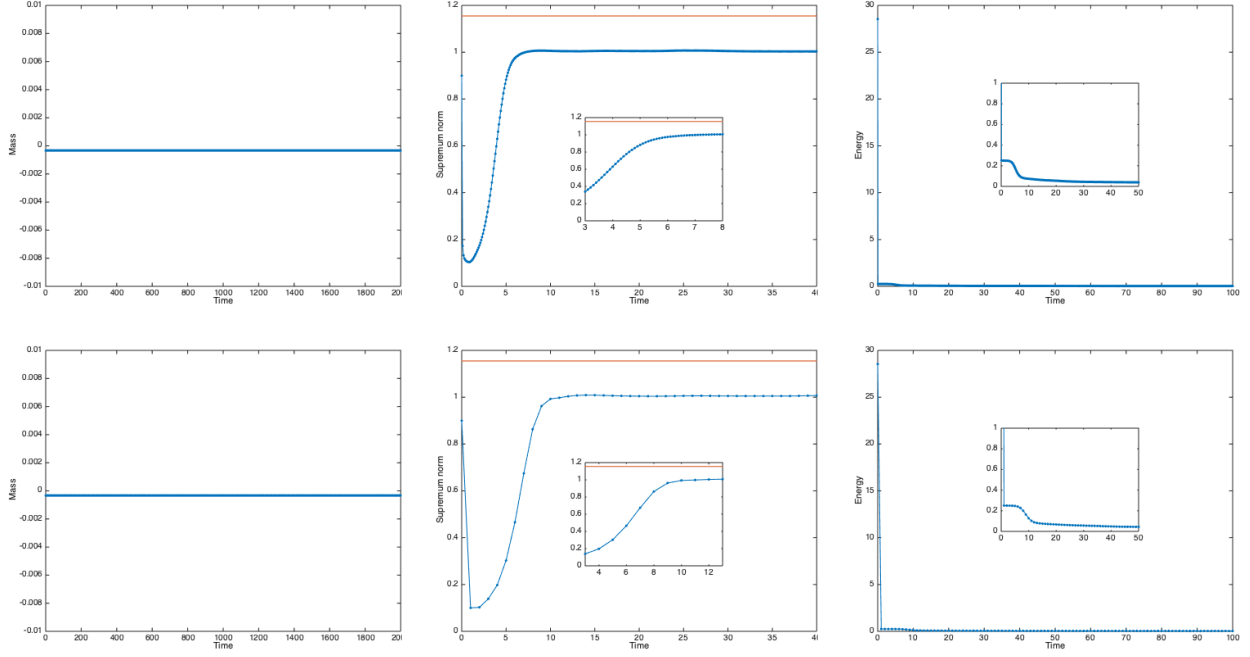


**Fig. 2** Evolutions of the mass (left), the supremum norm (middle) and the energy (right) with different time step sizes for the conservative Allen-Cahn equation (2.3) with the double-well potential in two dimensions. Top:  $\tau = 0.1$ ; bottom:  $\tau = 1$ .

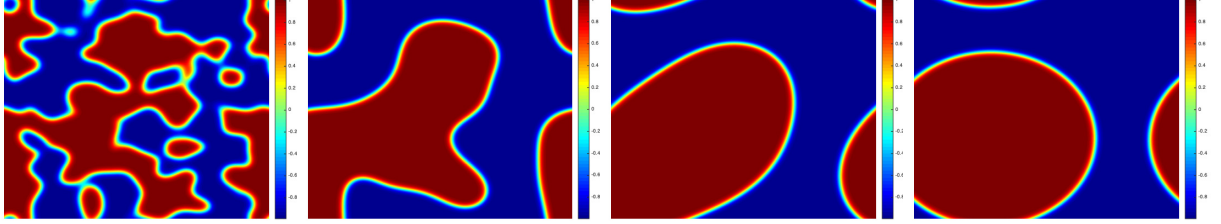


**Fig. 3** Simulated phase structures at  $t = 1, 10, 50, 300$  (from left to right) with  $\tau = 0.1$  for the Cahn-Hilliard equation (1.3) with the double-well potential in two dimensions.

Next we take  $f$  to be the Flory-Huggins potential function (2.8) with the parameters  $\theta = 0.8$  and  $\theta_c = 1.6$  in (2.8). According to Example 2, the positive root of  $f(\gamma) = f\left(-\sqrt{1 - \frac{\theta}{\theta_c}}\right)$  is  $\gamma = 0.986783601343632$  (numerical value) and the stabilizing coefficient is thus chosen as  $\kappa = 28.87$ . Figure 4 shows the configurations of the numerical solution at  $t = 1, 10, 50, 2200$  for the conservative Allen-Cahn equation with  $\tau = 0.1$  and  $\tau = 1$ . The corresponding evolutions of the mass, supremum norm and energy are presented in Figure 5, where the red line is  $\beta = \gamma \approx 0.9868$ . We observe that the mass is conserved and the energy decays monotonically. Moreover, the discrete MBP is preserved perfectly for the conservative Allen-Cahn equation where the solution is always located in the interval  $[-\beta, \beta]$ . Two simulations produced by different time step sizes again give us overall similar evolution processes. The results of the Cahn-Hilliard equation with  $\tau = 0.1$  are illustrated for  $t = 1, 10, 50, 800$  in Figure 6, where the almost same steady state as that of the conservative Allen-Cahn equation is reached but with a shorter time as expected.

### 5.2.2 Three-dimensional coarsening

Now we perform some three-dimensional simulations for the conservative Allen-Cahn equation (2.3) with  $\epsilon = 0.01$ . We use the spatial mesh size  $h = 1/256$  and the time step size  $\tau = 0.1$ .

We first simulate the case of the double-well potential function (2.7) and set the stabilizing coefficient  $\kappa = 3$  as before. Figure 7 shows the configuration of the numerical solution at  $t = 1, 30, 200, 4000$ . The

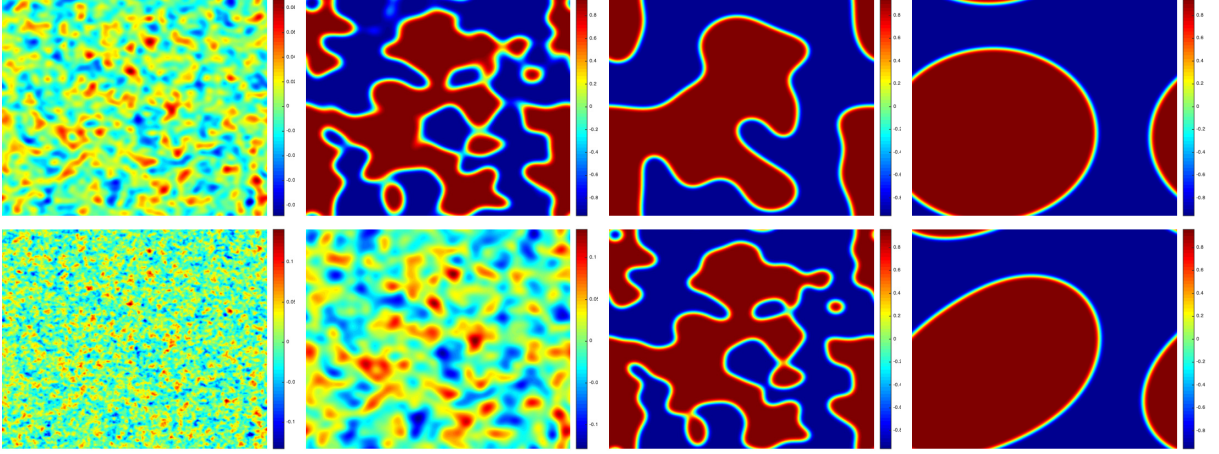


**Fig. 4** Simulated phase structures at  $t = 1, 10, 50, 2200$  (from left to right) with different time step sizes of the conservative Allen-Cahn equation (2.3) with the Flory-Huggins potential in two dimensions. Top:  $\tau = 0.1$ ; bottom:  $\tau = 1$ .

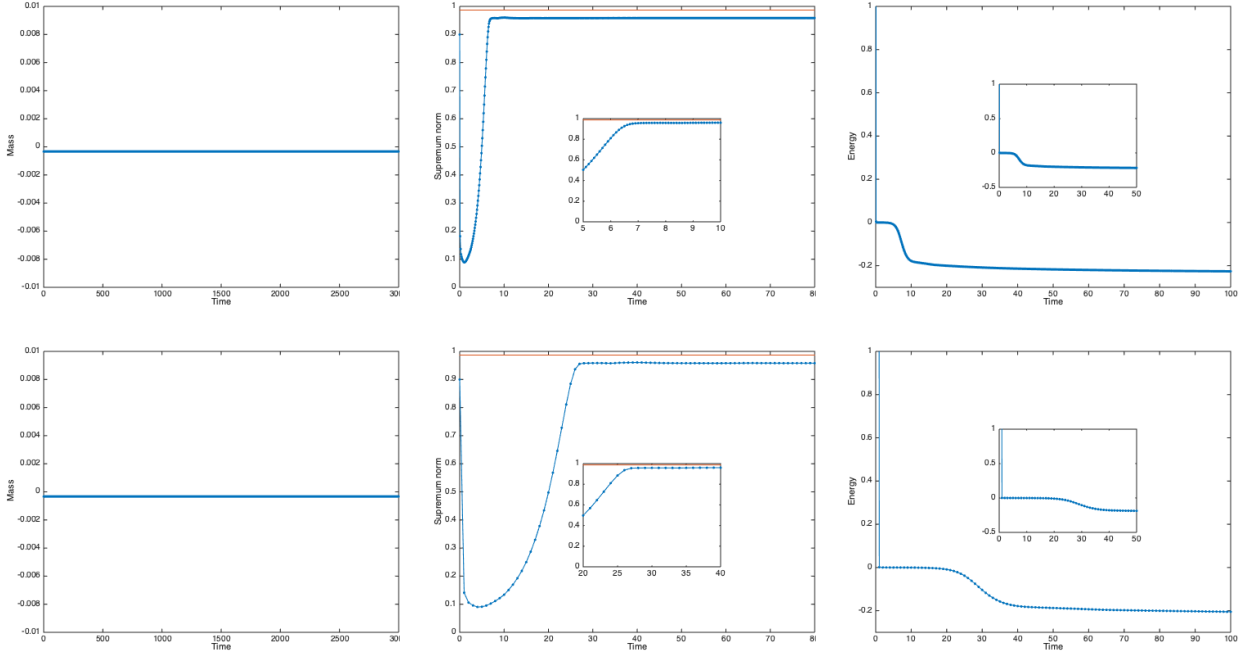


**Fig. 5** Evolutions of the mass (left), the supremum norm (middle) and the energy (right) for the conservative Allen-Cahn equation (2.3) with the Flory-Huggins potential in two dimensions. Top:  $\tau = 0.1$ ; bottom:  $\tau = 1$ .

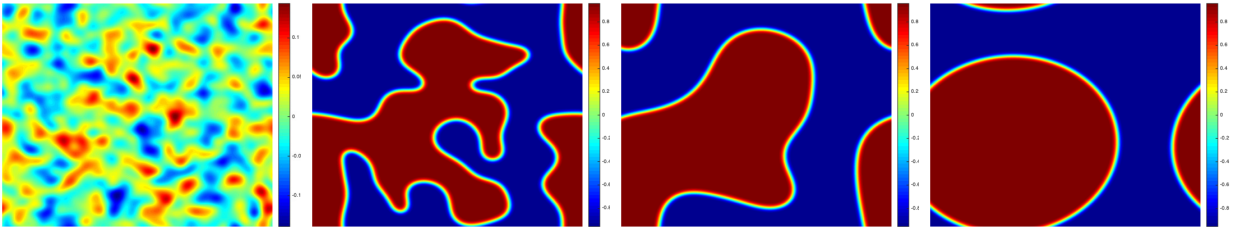


**Fig. 6** Simulated phase structures at  $t = 1, 10, 50, 800$  (from left to right) with  $\tau = 0.1$  for the Cahn-Hilliard equation (1.3) with the Flory-Huggins potential in two dimensions.

corresponding dynamics of the mass, the supremum norm and the energy are plotted in Figure 8, where

the red line is  $\beta = \frac{2}{3}\sqrt{3}$ . We observe that the mass is conserved and the energy decays monotonically along the time. Moreover, the MBP of the conservative Allen-Cahn equation is numerically preserved very well.

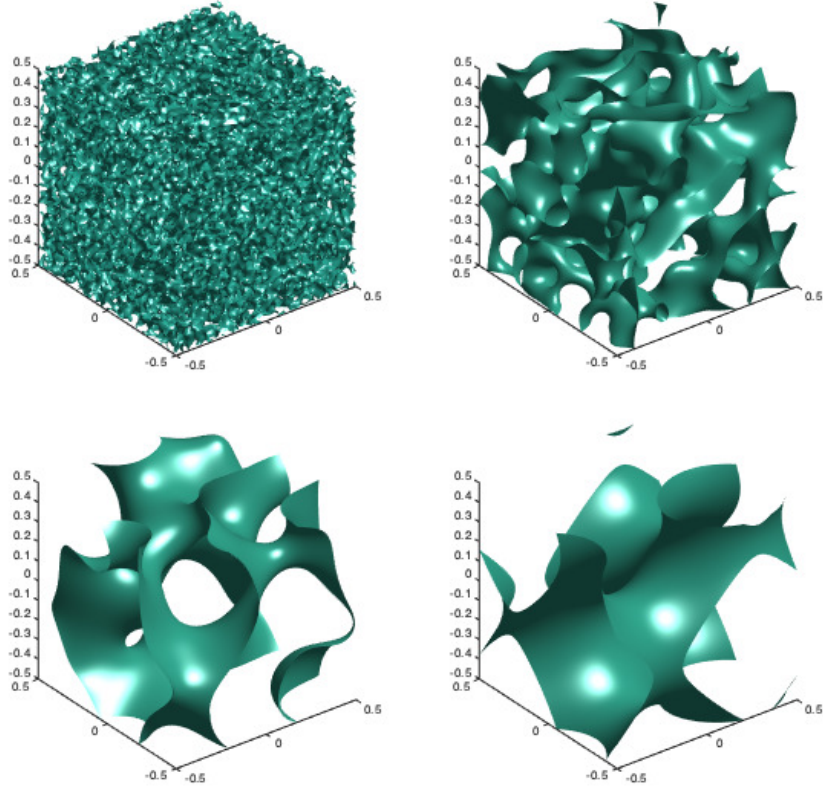


**Fig. 7** Simulated phase structures at  $t = 1, 30, 200, 4000$  (from left to right and top to bottom) with  $\tau = 0.1$  for the conservative Allen-Cahn equation (2.3) with the double-well potential in three dimensions.

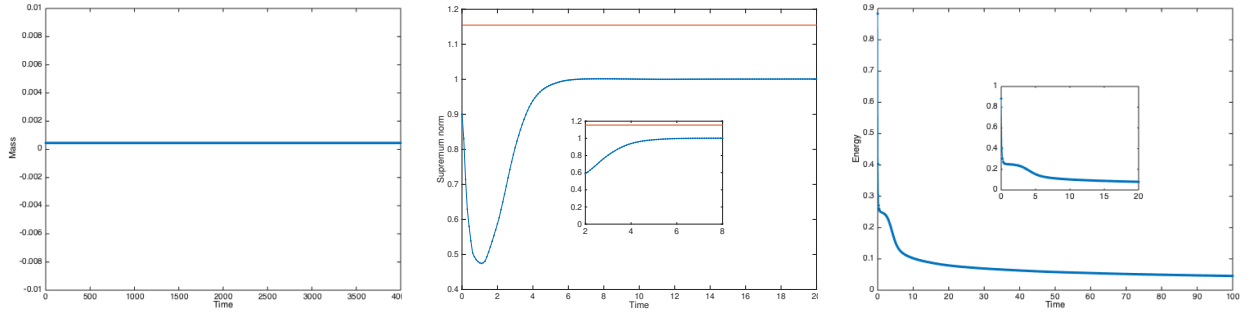


**Fig. 8** Evolutions of the mass (left), the supremum norm (middle) and the energy (right) for the conservative Allen-Cahn equation (2.3) with the double-well potential in three dimensions.

Next we solve the case of the Flory-Huggins potential function (2.8) in which the parameters are still  $\theta = 0.8$  and  $\theta_c = 1.6$ , and the stabilizing coefficient is again set to be  $\kappa = 28.87$ . Figure 9 shows the configuration of the numerical solution at  $t = 1, 30, 200, 4000$  and Figure 10 depicts how the mass, supremum norm and energy evolve in time, where the red line is  $\beta = \gamma \approx 0.9868$ . We again observe that the mass is conserved, the energy decays monotonically, and the MBP for the conservative Allen-Cahn equation (2.3) is numerically well-preserved.

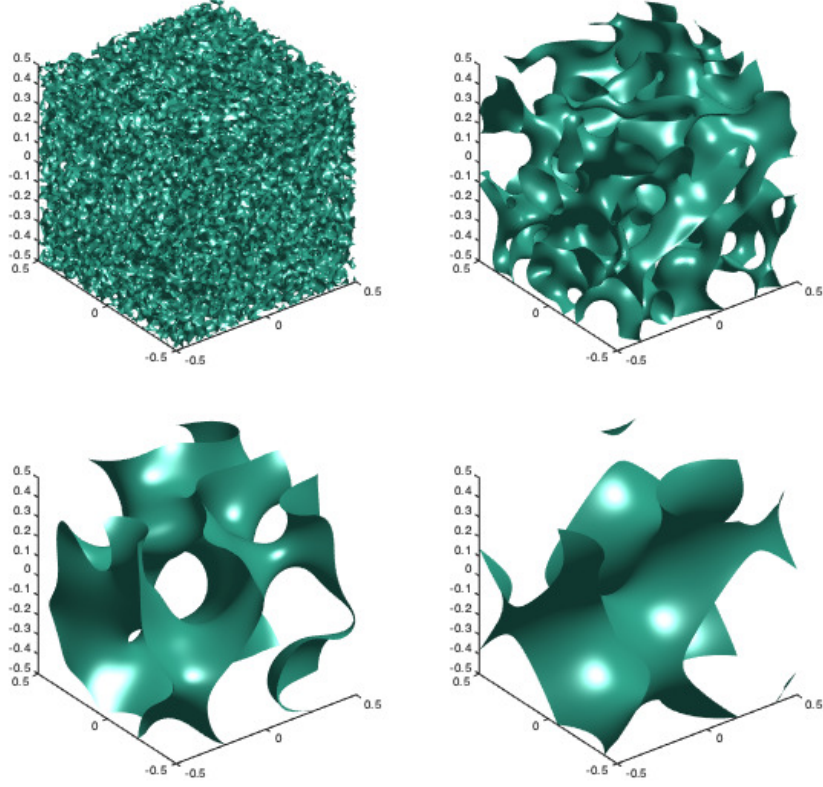


**Fig. 9** Simulated phase structures at  $t = 1, 30, 200, 4000$  (from left to right and top to bottom) with  $\tau = 0.1$  for the conservative Allen-Cahn equation (2.3) with the Flory-Huggins potential in three dimensions.

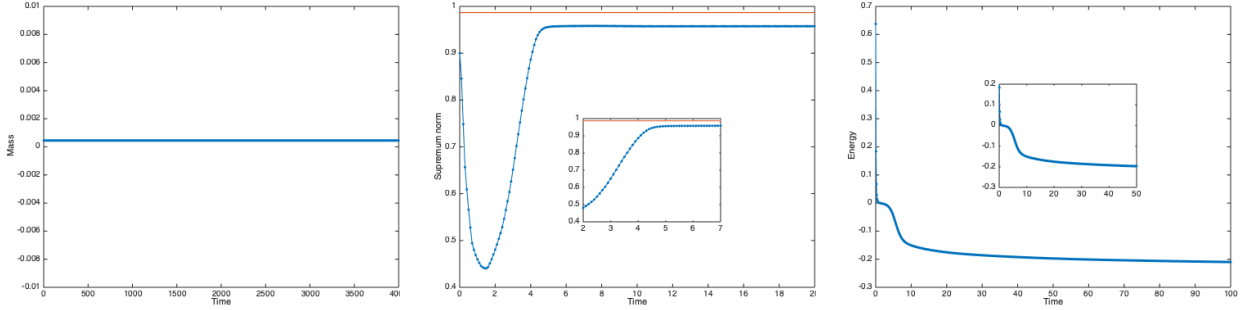


**Fig. 10** Evolutions of the mass (left), the supremum norm (middle) and the energy (right) for the conservative Allen-Cahn equation (2.3) with the Flory-Huggins potential in three dimensions.

### 5.3 The expanding bubble test

In this example, we numerically simulate the evolution of an expanding bubble in three dimensions, governed by the conservative Allen-Cahn equation (2.3) with  $\epsilon = 0.01$  and either the double-well potential function (2.7) or the Flory-Huggins potential function (2.8). The initial discontinuous configuration is given by

$$u_0(x, y, z) = \begin{cases} -0.5, & x^2 + y^2 + z^2 < 0.25^2, \\ 0.5, & \text{otherwise,} \end{cases}$$

which is illustrated in Figure 11. The radius of the bubble is expected to continuously increase until a steady state is reached. Again, we test the ETDRK2 scheme with the time step size  $\tau = 0.01$  and the spatial mesh size  $h = 1/256$ .

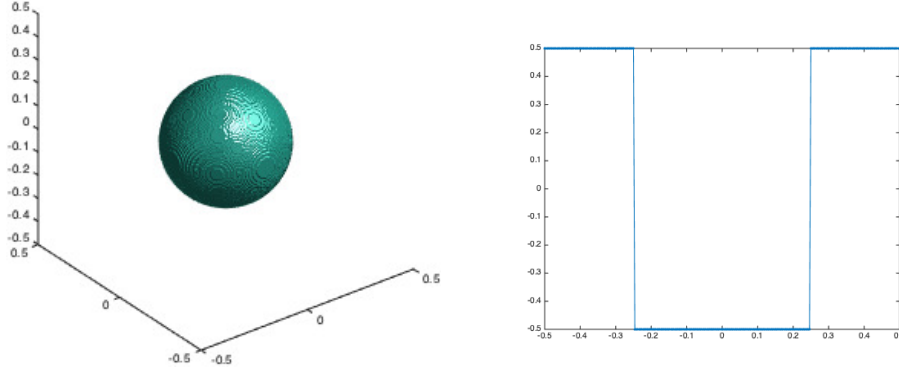


**Fig. 11** Initial configurations in the expanding bubble example. Left: the iso-surface; right: the cross-section view at  $x = 0$  and  $y = 0$ .

We first adopt the double-well potential function (2.7) with the stabilizing coefficient  $\kappa = 3$ . Figure 12 presents the expanding process of the bubble, in which the iso-surfaces ( $u = 0$ ) are plotted at the time  $t = 1, 10, 100$  respectively. Figure 13 shows the evolutions of the bubble radius, the mass, the supremum norm and the energy of the numerical solutions, where the red line is  $\beta = \frac{2}{3}\sqrt{3}$ . The radius of the bubble starts with 0.25 and gradually increases, and finally reaches a steady value around 0.4028. It is easy to find that the mass is conserved, the energy decays monotonically and the MBP is well preserved numerically along the time.

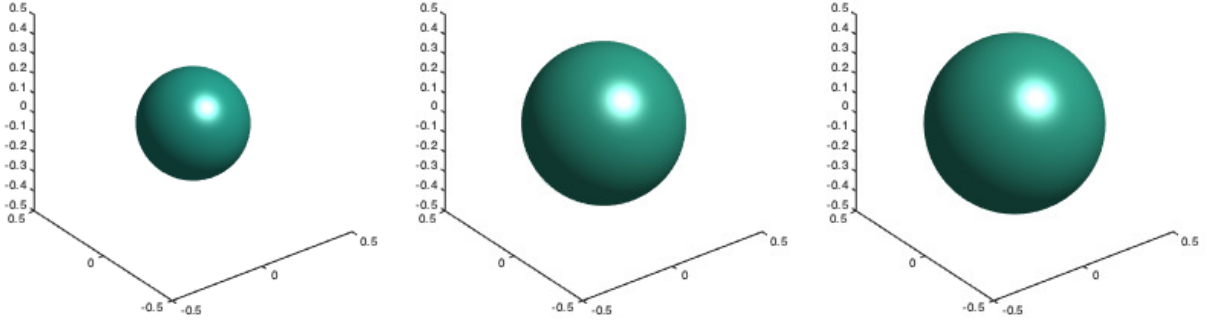


**Fig. 12** Simulated expanding bubbles at  $t = 1, 10, 100$  (from left to right) with  $\tau = 0.01$  for the conservative Allen-Cahn equation (2.3) with the double-well potential in three dimensions.

Next we take the Flory-Huggins potential function (2.8) with the stabilizing coefficient  $\kappa = 28.87$  to simulate the evolution of the bubble. The iso-surface views of the simulated bubble at  $t = 1, 4$  and  $100$  are given in Figure 14. Figure 15 presents the evolution of the bubble radius, the mass, the supremum norm and the energy of the numerical solutions, where the red line is  $\beta = 0.9868 \dots$ . The radius of the bubble starts with 0.25 and gradually increases to 0.4012 and reaches a steady state within a similar time period as the case of double-well potential. Again the mass is conserved, the energy decays monotonically and the MBP is well preserved numerically along the time.

## 6 Conclusions

In this paper we have developed and analyzed unconditional MBP-preserving linear numerical schemes (up to second order in time), the stabilized ETD1 and ETDRK2 schemes, for the conservative Allen-Cahn equation with nonlocal constraint. We generalize the framework of [12] on the MBP of semilinear

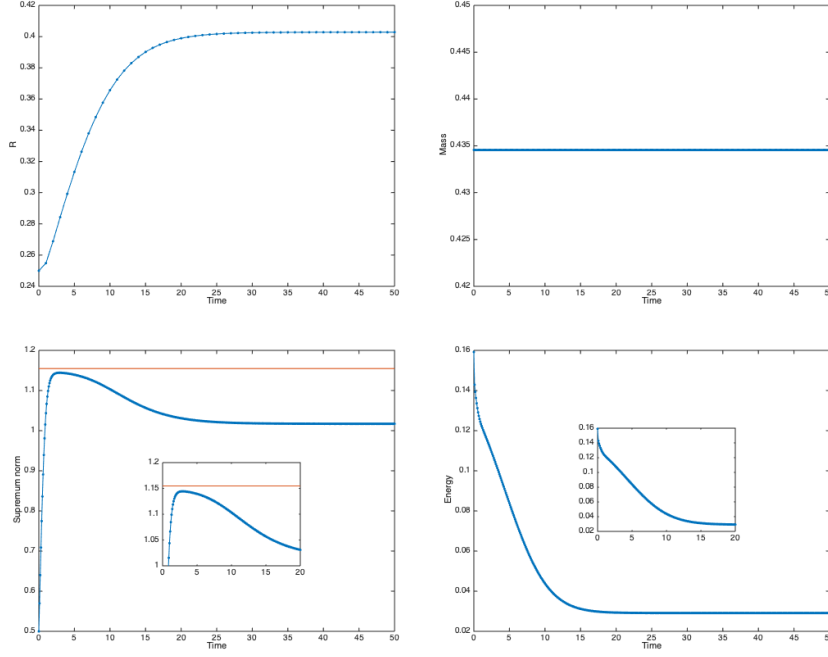


**Fig. 13** Evolutions of the radius (top-left), the mass (top-right), the supremum norm (bottom-left) and the energy (bottom-right) for the expanding bubble governed by the conservative Allen-Cahn equation (2.3) with the double-well potential in three dimensions.

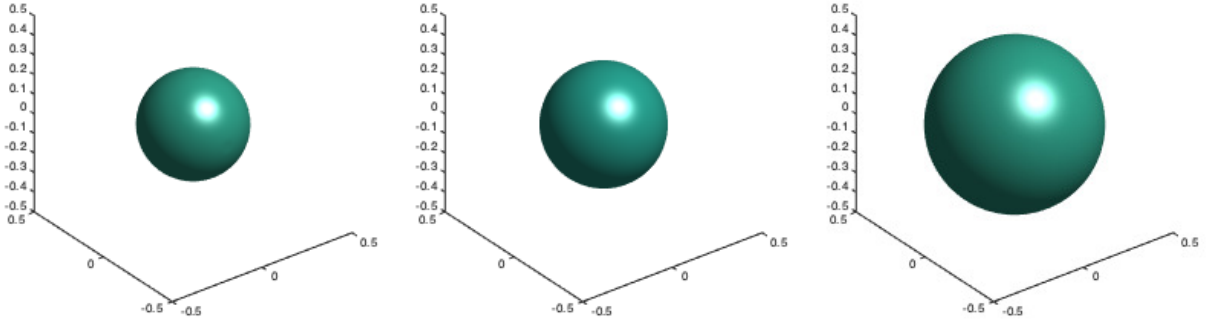


**Fig. 14** Simulated expanding bubbles at  $t = 1, 4$  and  $100$  (from left to right) with  $\tau = 0.01$  for the conservative Allen-Cahn equation (2.3) with the Flory-Huggins potential in three dimensions.

parabolic equations and corresponding ETD schemes to the conservative Allen-Cahn equation satisfying Assumption 1. The choice of the stabilizing coefficient plays an important role on designing unconditional MBP-preserving schemes and we note that the theoretically required stabilizing coefficient  $\kappa$  is obviously larger (especially for the case of Flory-Huggins potential) than that for the classic Allen-Cahn equation [11, 12]. It remains an open question whether a more delicate analysis can relieve such requirement. In addition, only the Laplace operator  $\Delta$  is considered in this paper, which generates contraction semigroup in  $C(\bar{\Omega})$  with suitable boundary conditions. However, many more general operators such as the second-order elliptic differential operator, the nonlocal diffusion operator [10] and the fractional Laplace operator [14] possess the similar property [12], and further studies are still needed on whether the above MBP analysis and the MBP-preserving schemes can be extended to those cases for the conservative Allen-Cahn equation.

It is also worth pointing out that, apart from the ETD methods, the integrating factor (IF) method is also an effective method to preserve the MBP conditionally or unconditionally, such as Runge-Kutta integrating factor (IFRK) schemes [19, 23]. They would be ideal potential candidates for designing higher-

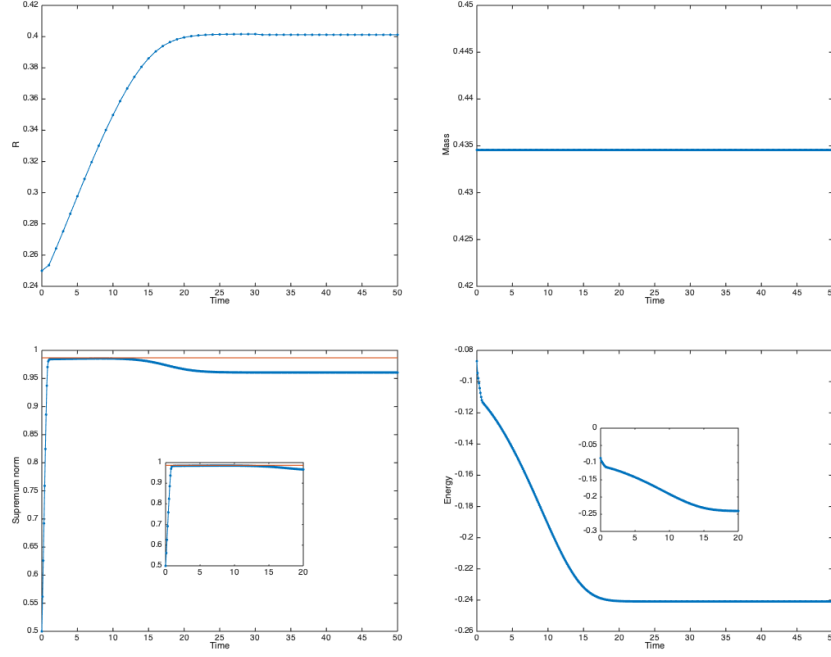


**Fig. 15** Evolutions of the radius (top-left), the mass (top-right), the supremum norm (bottom-left) and the energy (bottom-right) for the expanding bubble governed by the conservative Allen-Cahn equation (2.3) with the Flory-Huggins potential in three dimensions.

order accurate MBP-preserving numerical schemes. At the same time, extensions to the cases of complex-valued, vector-valued and matrix-valued conservative Allen-Cahn type dynamics are also subject to future investigation.

## References

1. Allen S M, Cahn J W. A microscopic theory for antiphase boundary motion and its application to antiphase domain coarsening. *Acta Metallurgica*, 1979, 27(6): 1085-1095.
2. Beylkin G, Keiser J M, Vozovoi L. A new class of time discretization schemes for the solution of nonlinear PDEs. *Journal of Computational Physics*, 1998, 147(2): 362-387.
3. Cahn J W, Hilliard J E. Free energy of a nonuniform system. I. Interfacial free energy. *Journal of Chemical Physics*, 1958, 28(2): 258-267.
4. Chen W, Wang C, Wang X, Wise S M. Positivity-preserving, energy stable numerical schemes for the Cahn-Hilliard equation with logarithmic potential. *Journal of Computational Physics: X*, 2019, 3: 100031.
5. Chen X, Hilhorst D, Logak E., Mass conserving Allen-Cahn equation and volume preserving mean curvature flow, *Interfaces and Free Boundaries*, 2010, 12: 527-549.
6. Copetti M I M, Elliott C M. Numerical analysis of the Cahn-Hilliard equation with a logarithmic free energy. *Numerische Mathematik*, 1992, 63(1): 39-65.
7. Cox S M, Matthews P C. Exponential time differencing for stiff systems. *Journal of Computational Physics*, 2002, 176(2): 430-455.
8. Debusche A, Dettori L. On the Cahn-Hilliard equation with a logarithmic free energy. *Nonlinear Analysis: Theory, Methods & Applications*, 1995, 24(10): 1491-1514.
9. Dong L, Wang C, Zhang H, Zhang Z. A positivity-preserving, energy stable and convergent numerical scheme for the Cahn-Hilliard equation with a Flory-Huggins-Degennes energy. *Communications in Mathematical Sciences*, 2019, 17(4): 921-939.
10. Du Q. *Nonlocal Modeling, Analysis, and Computation: Nonlocal Modeling, Analysis, and Computation*. Society for Industrial and Applied Mathematics, 2019.
11. Du Q, Ju L, Li X, Qiao Z. Maximum principle preserving exponential time differencing schemes for the nonlocal Allen-Cahn equation. *SIAM Journal on Numerical Analysis*, 2019, 57(2): 875-898.
12. Du Q, Ju L, Li X, Qiao Z. Maximum bound principles for a class of semilinear parabolic equations and exponential time differencing schemes. *arXiv preprint arXiv:2005.11465*, 2020.
13. Feng X, Prohl A. Numerical analysis of the Allen-Cahn equation and approximation for mean curvature flows. *Numerische Mathematik*, 2003, 94(1): 33-65.
14. Fernandez-Real X, Ros-Oton X. Boundary regularity for the fractional heat equation. *Revista de la Real Academia de Ciencias Exactas, Fisicasy Naturales. Serie A. Matematicas*, 2016, 110(1): 49-64.
15. Huang J, Ju L, Wu B. A fast compact time integrator method for a family of general order semilinear evolution equations. *Journal of Computational Physics*, 2019, 393: 313-336.

16. Hochbruck M, Ostermann A. Explicit exponential Runge–Kutta methods for semilinear parabolic problems. *SIAM Journal on Numerical Analysis*, 2005, 43(3): 1069-1090.
17. Lee D, Kim J. Comparison study of the conservative Allen-Cahn and the Cahn-Hilliard equations. *Mathematics and Computers in Simulation*, 2016, 119: 35-56.
18. Lee H G. High-order and mass conservative methods for the conservative Allen-Cahn equation. *Computers & Mathematics with Applications*, 2016, 72(3): 620-631.
19. Li J, Li X, Ju L, Feng X. Stabilized integrating factor Runge-Kutta method and unconditional preservation of maximum bound principle, submitted, 2020.
20. Li X, Ju L, Meng X. Convergence analysis of exponential time differencing schemes for the Cahn-Hilliard equation. *Communications in Computational Physics*, 2019, 26(5): 1510-1529.
21. Liao H, Tang T, Zhou T. A second-order and nonuniform time-stepping maximum-principle preserving scheme for time-fractional Allen-Cahn equations. *Journal of Computational Physics*, 2020, 414: 109473.
22. Ju L, Li X, Qiao Z, Zhang H. Energy stability and error estimates of exponential time differencing schemes for the epitaxial growth model without slope selection. *Mathematics of Computation*, 2018, 87(312): 1859-1885.
23. Ju L, Li X, Qiao Z, Yang J. Maximum bound principle preserving integrating factor Runge-Kutta methods for semilinear parabolic equations, arXiv preprint arXiv:2010.12165, 2020.
24. Ju L, Zhang J, Du Q. Fast and accurate algorithms for simulating coarsening dynamics of Cahn-Hilliard equations. *Computational Materials Science*, 2015, 108: 272-282.
25. Ju L, Zhang J, Zhu L. Fast explicit integration factor methods for semilinear parabolic equations. *Journal of Scientific Computing*, 2015, 62(2): 431-455.
26. Kim J, Lee S, Choi Y. A conservative Allen-Cahn equation with a space–time dependent Lagrange multiplier. *International Journal of Engineering Science*, 2014, 84: 11-17.
27. Peng G, Gao Z, Yan W, Feng X. A positivity-preserving nonlinear finite volume scheme for radionuclide transport calculations in geological radioactive waste repository. *International Journal of Numerical Methods for Heat & Fluid Flow*, 2019, 30(2): 516-534.
28. Peng G, Gao Z, Feng X. A stabilized extremum-preserving scheme for nonlinear parabolic equation on polygonal meshes. *International Journal for Numerical Methods in Fluids*, 2019, 90(7): 340-356.
29. Protter M H, Weinberger H F. Maximum principles in differential equations. Springer-Verlag New York, 1984.
30. Qian Y, Wang C, Zhou S. A positive and energy stable numerical scheme for the Poisson-Nernst-Planck-Cahn-Hilliard equations with steric interactions. *Journal of Computational Physics*, 2021, 426: 109908.
31. Rubinstein J, Sternberg P. Nonlocal reaction–diffusion equations and nucleation. *IMA Journal of Applied Mathematics*, 1992, 48(3): 249-264.
32. Shen J, Tang T, Yang J. On the maximum principle preserving schemes for the generalized Allen-Cahn equation. *Communications in Mathematical Sciences*, 2016, 14(6): 1517-1534.
33. Shen J, Xu J. Unconditionally bound preserving and energy dissipative schemes for a class of Keller–Segel equations. *SIAM Journal on Numerical Analysis*, 2020, 58(3): 1674-1695.
34. Shen J, Xu J, Yang J. A new class of efficient and robust energy stable schemes for gradient flows. *SIAM Review*. 2019, 61(3):474-506.
35. Shen, J, Yang, X. Numerical approximations of Allen-Cahn and Cahn-Hilliard equations. *Discrete & Continuous Dynamical Systems-A*, 2010, 28 (4) : 1669-1691.
36. Shin J, Park S K, Kim J. A hybrid FEM for solving the Allen-Cahn equation. *Applied Mathematics and Computation*, 2014, 244: 606-612.
37. Tang T, Yang J. Implicit-explicit scheme for the Allen-Cahn equation preserves the maximum principle. *Journal of Computational Mathematics*, 2016, 34(5): 471-481.
38. Xiao X, Feng X, Yuan J. The stabilized semi-implicit finite element method for the surface Allen-Cahn equation. *Discrete & Continuous Dynamical Systems-B*, 2017, 22(7): 2857.
39. Xiao X, Feng X, He Y. Numerical simulations for the chemotaxis models on surfaces via a novel characteristic finite element method. *Computers & Mathematics with Applications*, 2019, 78(1): 20-34.
40. Xiao X, He R, Feng X. Unconditionally maximum principle preserving finite element schemes for the surface Allen-Cahn type equations. *Numerical Methods for Partial Differential Equations*, 2020, 36(2): 418-438.
41. Xiao X, Dai Z, Feng X. A positivity preserving characteristic finite element method for solving the transport and convection-diffusion-reaction equations on general surfaces. *Computer Physics Communications*, 2020, 247: 106941.
42. Xu C, Tang T. Stability analysis of large time-stepping methods for epitaxial growth models. *SIAM Journal on Numerical Analysis*, 2006, 44(4): 1759-1779.
43. Yang J, Du Q, Zhang W. Uniform  $L^p$ -bound of the Allen-Cahn equation and its numerical discretization. *International Journal of Numerical Analysis & Modeling*, 2018, 15:213-227.
44. Yang X, Zhang G. Numerical approximations of the Cahn-Hilliard and Allen-Cahn equations with general nonlinear potential using the Invariant Energy Quadratization approach. arXiv preprint arXiv:1712.02760. 2017.
45. Zhai S, Weng Z, Feng X. Investigations on several numerical methods for the nonlocal Allen-Cahn equation. *International Journal of Heat and Mass Transfer*, 2015, 87: 111-118.
46. Zhai S, Weng Z, Feng X. Fast explicit operator splitting method and time-step adaptivity for fractional nonlocal Allen-Cahn model. *Applied Mathematical Modeling*, 2016, 40(2): 1315-1324.
47. Zhang J, Yang X. Numerical approximations for a new  $L^2$ -gradient flow based phase field crystal model with precise nonlocal mass conservation. *Computer Physics Communications*, 2019, 243: 51-67.
48. Zhang J, Yang X. Unconditionally energy stable large time stepping method for the  $L^2$ -gradient flow based ternary phase-field model with precise nonlocal volume conservation. *Computer Methods in Applied Mechanics and Engineering*, 2020, 361: 112743.
49. Zhang J, Chen C, Yang X, Chu Y, Xia Y. Efficient, non-iterative, and second-order accurate numerical algorithms for the anisotropic Allen-Cahn Equation with precise nonlocal mass conservation. *Journal of Computational and Applied Mathematics*, 2020, 363: 444-463.